minerals

MDPI

Article

The Trace-Element Characteristics of Chrysoberyl: Insights from Compositional and Spectroscopic Analyses

Linling Dong [1,2,*], Yimiao Liu [1], Xinxin Gao [1] and Ren Lu [1,*]

[1] Gemmological Institute, China University of Geosciences, Wuhan 430074, China; yim2015@163.com (Y.L.); gaoxinxin@cug.edu.cn (X.G.)
[2] School of Jewelry, West Yunnan University of Applied Sciences, Baoshan 679100, China
* Correspondence: sarah1053839869@cug.edu.cn (L.D.); renlu.cc@gmail.com (R.L.)

Abstract: To characterize the trace-element characteristics of chrysoberyl, we studied twenty-six chrysoberyl samples from various localities by using laser ablation inductively coupled plasma mass spectrometry (LA–ICP–MS), photoluminescence (PL), and ultraviolet–visible–near-infrared (UV–Vis–NIR) spectroscopy. Chemical analysis has confirmed the existence of trace elements, including Fe, Ti, Ga, Sn, B, Cr, and V. The phenomenon of ionic isomorphic substitution frequently occurs at lattice sites within chrysoberyl. Notably, the isomorphic substitution of Al^{3+} in octahedral sites is significant, with the primary substituting elements being Fe, Ti, Cr, V, Ga, and Sn. The PL spectra of chrysoberyl samples exhibit sharp peaks at 678 and 680 nm, which are attributed to Cr^{3+}, even in samples in which the Cr concentration is below the detection limit of LA-ICP-MS. This demonstrates the high-sensitivity feature of PL spectroscopy. The UV–Vis–NIR spectra of chrysoberyl samples consistently exhibit a band at 440 nm, and strong double narrow bands near 367 nm and 375 nm are observed. These spectral features are associated with Fe^{3+} chromophores—specifically, Fe^{3+}-Fe^{3+} pairs or clusters and Fe^{3+} ions, respectively. By combining LA–ICP–MS analysis and PL mapping on a sample exhibiting color zoning, it has been found that the darker sections contain a higher concentration of Cr compared to the lighter sections, while the concentrations of other elements remain largely consistent. In other words, subtle variations in Cr concentration may be the underlying cause of color zoning in chrysoberyl.

Keywords: trace elements; chrysoberyl; photoluminescence

check for updates

Citation: Dong, L.; Liu, Y.; Gao, X.; Lu, R. The Trace-Element Characteristics of Chrysoberyl: Insights from Compositional and Spectroscopic Analyses. *Minerals* **2024**, *14*, 1280. https://doi.org/10.3390/min14121280

Academic Editor: Stefanos Karampelas

Received: 12 November 2024
Revised: 12 December 2024
Accepted: 13 December 2024
Published: 17 December 2024

Copyright: © 2024 by the authors. Licensee MDPI, Basel, Switzerland. This article is an open access article distributed under the terms and conditions of the Creative Commons Attribution (CC BY) license (https://creativecommons.org/licenses/by/4.0/).

1. Introduction

Chrysoberyl ($BeAl_2O_4$) is an orthorhombic mineral belonging to the *Pnma* space group and is recognized as one of the traditional and noted colorful gemstones. In its purest form, chrysoberyl is colorless and transparent. However, when doped with trace impurity elements, colorless chrysoberyl can exhibit a variety of hues, including yellow, orange–yellow, and yellow–green. Compared to alexandrite, chrysoberyl exhibits a purer composition in terms of trace elements [1]. Previously, the rare varieties of chrysoberyl, such as cat's eye and alexandrite, have been the focus of attention [2–5]. In addition to its special optical phenomena, the natural body color and intrinsic physical properties of chrysoberyl have laid a solid foundation for its status as a gemstone-grade mineral. However, the common varieties of chrysoberyl have only received limited attention.

The color of chrysoberyl is primarily attributed to trace amounts of transition metal ions. Specifically, trace Fe^{3+} ions are responsible for the yellow hue in chrysoberyl, while Cr^{3+} ions cause the color-change effect [6]. Samples of chrysoberyl and alexandrite from the Manyara Lake deposit in Tanzania contain Fe, Cr, and V, with significant variations in their concentrations. Elements such as B, Mg, Ga, Sn, and Ge, among others, are considered useful for determining the origin of these gemstones [2]. The majority of gemstone varieties within the chrysoberyl family are chrysoberyl itself, with Fe^{3+} being

the primary trace element, accompanied by minor amounts of metal ions such as Mg^{2+}, Cr^{3+}, and V^{3+} [3]. A study using Proton-Induced X-ray Emission (PIXE) technology was conducted on natural chrysoberyl samples sourced from the Eastern Ghats of India. Sixteen elements were identified in these chrysoberyl samples, including Al, Cr, Ti, V, Cu, Fe, Pb, Mo, La, and Ce [7]. Chemical analysis of chrysoberyl using Energy-Dispersive X-ray Fluorescence (EDXRF) suggests that V and Cr components are relatively scarce, while iron is abundant [8]. In summary, current research on trace elements in chrysoberyl is largely qualitative and lacks systematic investigation. A detailed study of the compositional variations in chrysoberyl is also lacking.

The characteristics of trace elements are crucial for studying the physical and color properties of minerals. In this study, we investigated the trace element composition of chrysoberyl samples sourced from various localities, including Sri Lanka, Tanzania, Brazil, and India. The primary objectives of this research were to characterize the trace element signatures and compositional relationships within chrysoberyl, analyze the correlations between crystal color and photoluminescent characteristics, explore the roles of trace elements in photoluminescence and coloration, and further investigate the application of trace element detection techniques and methodologies.

2. Materials and Methods

Samples. This study includes a total of twenty-six chrysoberyl samples, with colors ranging from greenish-yellow to yellow. Among them, the natural chrysoberyl samples from Mogok, Myanmar, were kindly provided by mineral and gem collector Mr. Min Lwin from Myanmar. The natural chrysoberyl samples originating from Sri Lanka, Tanzania, Brazil, and India were purchased from gemstone dealers (Figure 1). All samples were initially obtained as rough gemstones and were subsequently prepared as doubly polished wafers, oriented parallel to the crystallographic axis to facilitate precise spectral acquisition.



Figure 1. Rough and polished chrysoberyl samples from various localities: (**A**) Myanmar; (**B**) Sri Lanka; (**C**) Tanzania; (**D**) India; (**E**) Brazil.

Trace Element Analysis. Laser ablation–inductively coupled plasma–mass spectrometry (LA–ICP–MS) analysis was performed using the Agilent 7500 ICP–MS combined with a GeoLas 193 nm laser at the Wuhan Sample Solution Analytical Technology Co., Ltd., Wuhan, China. Ablation conditions were a 6 Hz repetition rate, 3.5 J/cm^2 fluence, and a laser spot size of 44 μm. The quantitative calibration standards of the National Institute of Standards and Technology (NIST) glass SRM 610, SRM 612, and U.S. Geological Sur-

vey (USGS) synthetic glasses BCR-2G, BHVO-2G, and BIR-1G [9] were used as reference materials. Each analysis was normalized by aluminum ions. A time-drift correction was then applied using linear interpolation (with time) for every nine analyses according to the variations of SRM 610. Offline selection, integration of background, analyte signals, and quantitative calibration were carried out using ICPMSDataCal [10]. The testing points for the samples were selected in internally clean, color-uniform areas, with three points randomly chosen from each sample for LA–ICP–MS testing to ensure the reliability of the experimental data.

The units adopted for LA–ICP–MS test data are weight percentage (wt.%) and parts per million by weight (ppmw), indicating the mass of the elements. In chemical analyses, such trace element data are usually directly used for comparison. However, when analyzing the crystallochemical characteristics of the samples, this study converts the weight percentages (wt.%) and parts per million by weight (ppmw) of major and some trace elements measured by LA-ICP-MS into atoms per formula unit (apfu), i.e., apfu = (molecular weight of $BeAl_2O_4$)/(atomic weight of the element $\times$ 10^6) $\times$ ppmw. Using apfu instead of weight percentages is more suitable for analyzing the crystallochemical characteristics of chrysoberyl. When analyzing the gemstone coloration mechanism, it is necessary to convert the ppmw into ppma using ppma = (molecular weight of $BeAl_2O_4$)/7/(atomic weight of the element) $\times$ ppmw modified from Emmett [11].

Photoluminescence (PL) Spectroscopy. Photoluminescence spectroscopy was performed by the JASCO NRS-7500 spectrometer system with a Peltier-cooled CCD detector and a high-resolution built-in CMOS camera (Gemmological Institute of China University of Geosciences (Wuhan)). Polarized photoluminescence spectra were excited by a green diode laser (532 nm) with a power of 4.8 mW. A 520.6 cm^{-1} silicon wafer was used for spectral calibration. Spectra in the range of 670–700 nm were collected in confocal mode using a 50$\times$ objective and were dispersed by a diffraction grating with 1800 grooves per mm. The exposure time of 0.5 s per frame and 2 accumulation times were used to improve the signal-to-noise ratio. When collecting spectra, it is advisable to select areas with good polishing quality, internal cleanliness, and uniform color as much as possible. All the samples were measured under the same conditions.

To gain deeper insight into the distribution of photoluminescence related to its trace elements, a PL mapping of sample S3 was also conducted using a JASCO NRS-7500 spectrometer equipped with a 532 nm laser. A PL mapping image is generated by moving the sample on a fast X–Y stage scan while storing the digitized values of the spectrum at each point, with a 20-micrometer interval between each point and each point being tested twice.

UV–Vis–NIR Spectroscopy. To collect the main chromophore features and illustrate the quantitative relationship between trace elements and spectral absorption, doubly polished wafers were analyzed with ultraviolet/visible/near-infrared (UV–Vis–NIR) spectroscopy using a JASCO MSV-5200 spectrometer equipped with a microscope and a 16$\times$ objective (Gemmological Iinstitute of China University of Geosciences (Wuhan)). The test zone of 400 μm diameter is close to the laser spots resulting from laser ablation inductively coupled plasma-mass spectrometry (LA–ICP–MS) analysis. Spectra were collected in the 300–1000 nm range. The spectral resolution was 0.1 nm with a scan speed of 100 nm/min. Perform baseline correction on the spectra and convert the vertical axis unit of the spectral data to an absorption coefficient (α, cm^{-1}) using the conversion formula α = 2.303 A/t, where A represents absorbance and t is the path length in centimeters. This conversion is to eliminate the influence of sample thickness on absorption [12].

3. Results

3.1. Chemical Analysis

The chemical analyses of major and trace elements in these samples were conducted using LA–ICP–MS. Each sample was analyzed at three separate points to obtain an average value. Additionally, the samples from each locality were analyzed to obtain both a range

and an average, respectively. The data are presented in units of ppmw and ppma, respectively, to facilitate subsequent analysis of origin characteristics and research into the causes of coloration.

The generalized trace element profiles are presented in Table 1. The results indicate that the main trace elements of chrysoberyl are Fe (7867–41,749 ppmw), Ti (22–3274 ppmw), Ga (296–1802 ppmw), and Sn (35–2495 ppmw), with low concentrations of B, Cr, and V.

Table 1. Trace elements of chrysoberyl samples in ppmw.

		B	Fe	Ti	Cr	V	Ga	Sn
Myanmar	**M1**	32	12,302	138	Bdl *	3	328	1747
	M2	49	19,324	22	bdl	3	374	264
	M3	59	24,624	513	bdl	5	772	383
	M4	39	8085	258	bdl	11	340	1962
	M5	110	40,178	87	bdl	bdl	505	633
	M6	67	35,885	2378	bdl	bdl	367	728
	Range	**32–110**	**8085–40,178**	**22–2378**	**bdl**	**bdl-11**	**328–772**	**264–1962**
	Average	**59**	**23,400**	**566**	**bdl**	**4**	**448**	**953**
Sri Lanka	**S1**	44	9250	1095	bdl	13	1156	98
	S2	34	8651	54	bdl	bdl	1480	150
	S3	39	11,800	266	bdl	bdl	1249	705
	S4	35	18,597	2314	bdl	3	1190	1508
	S5	30	10,289	2020	bdl	11	1134	54
	Range	**30–44**	**8651–18,597**	**54–2314**	**bdl**	**bdl-13**	**1134–1480**	**54–1508**
	Average	**36**	**11,717**	**1150**	**bdl**	**5**	**1242**	**503**
Tanzania	**T1**	20	11,495	231	37	20	527	35
	T2	54	22,755	29	bdl	bdl	1205	253
	T3	14	41,749	3274	bdl	6	396	1607
	T4	85	8482	187	bdl	bdl	296	532
	T5	83	8742	43	bdl	bdl	779	142
	T6	24	7867	1923	5	10	891	231
	Range	**14–85**	**7867–41,749**	**29–3274**	**bdl-37**	**bdl-20**	**296–1205**	**35–1607**
	Average	**47**	**16,848**	**948**	**7**	**6**	**682**	**467**
India	**I1**	12	16,925	433	11	17	419	67
	I2	bdl	15,476	427	11	23	377	100
	I3	18	17,075	556	7	18	392	139
	I4	11	16,352	466	7	19	385	85
	I5	19	16,143	250	17	19	412	54
	I6	bdl	17,659	690	11	20	423	153
	Range	**bdl-19**	**15,476–17,659**	**250–690**	**7–17**	**17–23**	**385–423**	**54–153**
	Average	**10**	**16,605**	**470**	**11**	**19**	**401**	**100**
Brazil	**B1**	24	12,021	1386	bdl	2	1802	2495
	B2	31	12,481	2147	bdl	bdl	1205	460
	B3	17	16,222	1198	bdl	4	1386	2081
	Range	**17–31**	**12,021–16,222**	**1198–2147**	**bdl**	**bdl-4**	**1205–1802**	**460–2495**
	Average	**24**	**13,574**	**1577**	**bdl**	**2**	**1464**	**1679**

* bdl = below the detection limit of the LA-ICP-MS analysis.

3.2. Photoluminescence Features

To investigate the luminescence features, PL spectra were acquired for chrysoberyl samples. In summary, the intensity of the PL spectrum augments with an increase in Cr concentration, as illustrated in Figure 2A. Notably, even samples with Cr concentrations below the detection limit of LA–ICP–MS exhibit discernible PL spectra attributed to Cr, as shown in Figure 2B. This demonstrates that PL possesses higher sensitivity compared to LA–ICP–MS for detecting Cr in these samples. The spectra exhibit a characteristic intensive doublet. By correlating the PL spectra with previous literature data [13–15], the sharp peaks

observed at 678 and 780 nm were assigned to Cr^{3+} ions, corresponding to the R_{2m} and R_{1m} lines associated with Cr ions occupying mirror sites within the chrysoberyl structure.

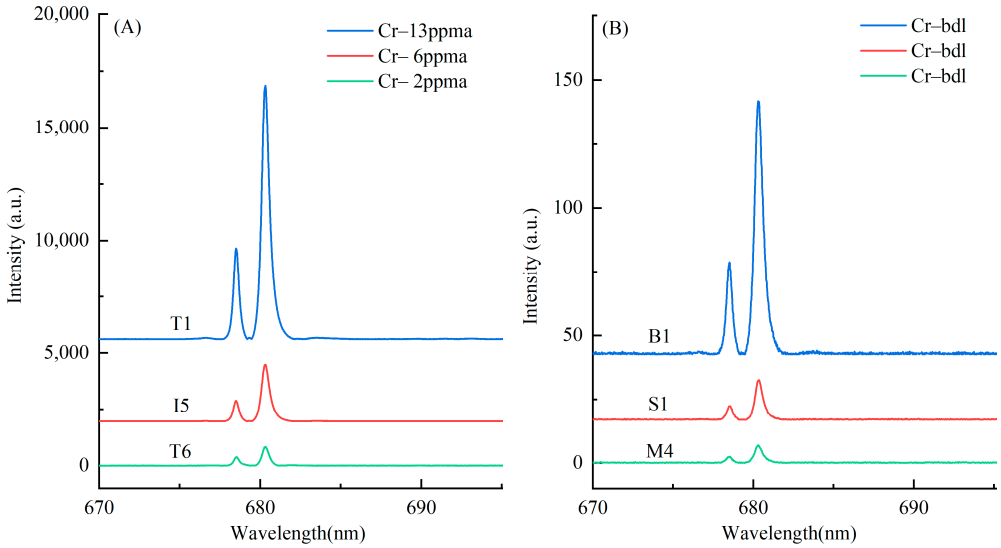


Figure 2. The photoluminescence spectra of chrysoberyl samples. The spectral directions are in the same orientation. (**A**) Increasing Cr concentration; (**B**) Cr concentrations below the detection limit of LA-ICP-MS.

3.3. UV–Vis–NIR Features

To collect the main chromophore features, UV–Vis–NIR spectra were acquired for chrysoberyl samples. Notable absorption features include a band at 440 nm, weak broad bands near 500 nm, and strong double narrow bands centered at 367 nm and 375 nm. Prior literature has attributed the color of chrysoberyl to Fe^{3+} [1,3,6,8,13], yet the specific assignment of these bands in the absorption spectrum remained ambiguous. By comparing with the iron-bearing corundum, which has a similar crystal structure, it is plausible to speculate that the peaks at 367 nm and the broadband near 500 nm in Fe-bearing chrysoberyl are attributed to Fe^{3+}-Fe^{3+} pairs, while the peak at 375 nm is assigned to the Fe^{3+} ion in chrysoberyl [12,16]. Furthermore, the band near 440 nm is attributed to Fe^{3+}-Fe^{3+} pairs or clusters [17]. Thus, Fe^{3+} chromophores may be responsible for the greenish-yellow hue observed in chrysoberyl. As illustrated in Figure 3, the absorption coefficient of the iron chromophore is dependent on the iron concentration, with the absorption coefficient increasing as the iron concentration rises.

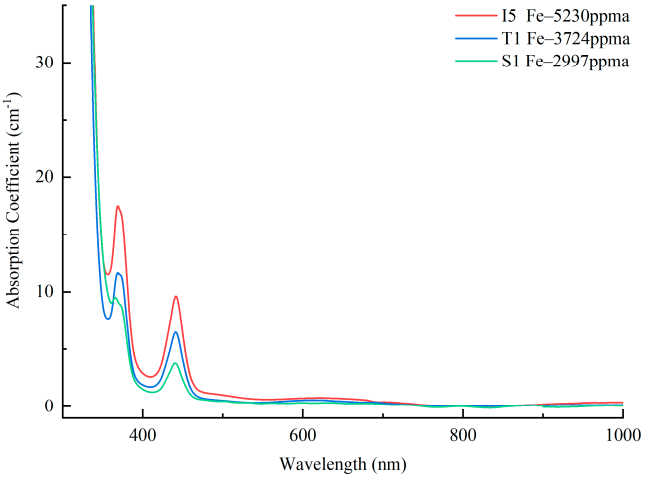


Figure 3. The UV–Vis–NIR spectra of chrysoberyl samples. The spectral directions are in the same orientation.

4. Discussion

4.1. Chemical and Provenance Features

To investigate the similarities and differences in chrysoberyl from various localities, the diagrams (Figure 4) are plotted using chemical data in Table 1. Figure 4 demonstrates that, apart from the relatively distinct characteristics of chrysoberyl from India, the data for samples from other origins overlap and are difficult to distinguish. Separating them may require a larger sample size and a more extensive sampling strategy. The composition of trace elements in samples from different localities varies slightly and exhibits their respective characteristics: Fe—present at very high levels in all samples, which is generally consistent with previous research findings [18,19]. Myanmar samples exhibit a higher concentration of Fe, averaging 23,400 ppmw, while chrysoberyl samples from Sri Lanka have a lower concentration of Fe. Chrysoberyl samples from different localities exhibit relatively wide variations in iron content, particularly those from Myanmar and Tanzania. Chrysoberyl with higher iron content is typically of metamorphic origin, whereas magmatic chrysoberyl samples found in leucogranites and pegmatites generally have lower iron content [20]. Therefore, it can be inferred that the majority of the chrysoberyl samples in this study belong to the metamorphic origin (>9370 ppmw Fe [20]). Ti—Sri Lankan and Brazilian stones have relatively high Ti concentrations, while Indian and Myanmar samples have lower Ti concentrations. Ga—Brazilian and Sri Lankan stones have a higher gallium concentration, which is two to three times higher than those from other localities; Sn—Brazilian chrysoberyl samples exhibit the highest Sn concentrations, while Indian samples have the lowest amounts. B—Myanmar stones have a higher B concentration, and Indian chrysoberyl samples have lower B concentrations; Cr, V—very low, being one to four orders of magnitude lower than those of other trace elements and even below the detection limits of LA–ICP–MS. The Cr and V are also very important in distinguishing Indian and Tanzanian chrysoberyl samples from those of other localities. Among them, Indian and Tanzanian chrysoberyl samples have higher Cr and V concentrations (see Figure 4D).

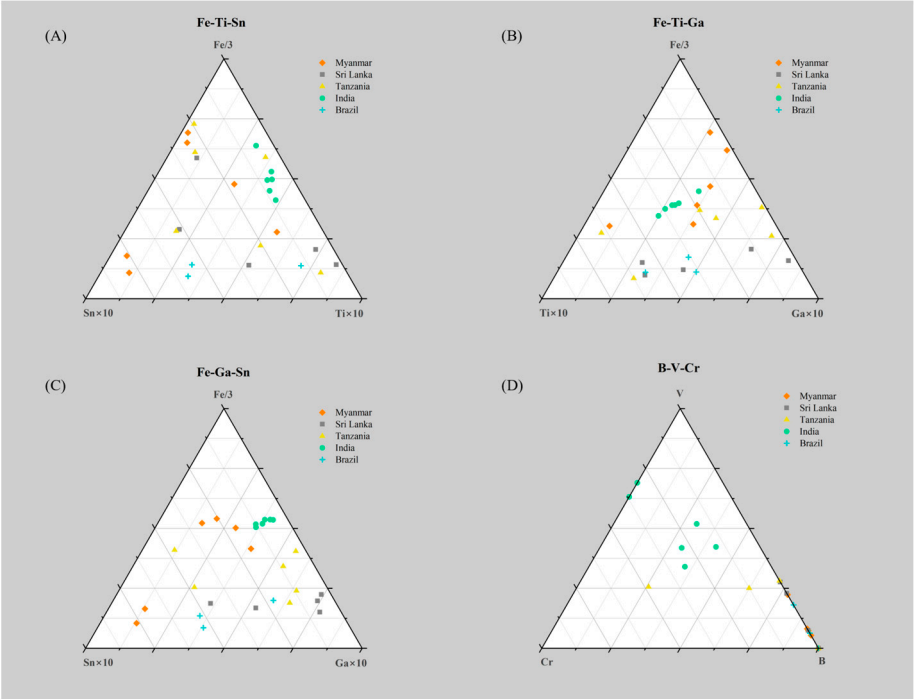


Figure 4. The elemental ternary plots illustrate the relationships between chemical composition and origins. (**A**) The Fe-Ti-Sn diagram; (**B**) The Fe-Ti-Ga diagram; (**C**) The Fe-Ga-Sn diagram; (**D**) The B-V-Cr diagram.

4.2. Characteristics of Ionic Substitutions in the Crystal Lattice Sites

The phenomenon of isomorphic substitution of ions frequently occurs within the crystal lattice sites of chrysoberyl [21]. Notably, Al^{3+}, which is octahedrally coordinated, undergoes significant isomorphic substitution. An approximate linear negative correlation is observed between the concentration of Al and the concentration of metal ions (denoted as Me^{n+}) being approximately 2 apfu (atoms per formula unit), as illustrated in Figure 5. Here, "Me^{n+}" primarily encompasses trace elements such as Fe, Ti, Ga, Sn, Cr, and V, suggesting that the octahedral-coordinated Al is predominantly substituted by these Me^{n+} metal ions.

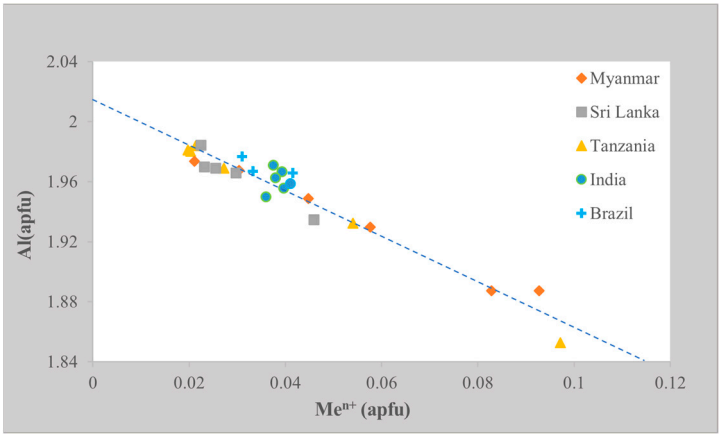


Figure 5. An approximate linear negative correlation between the content of Al and the content of octahedral-site substituting metal ions (Me^{n+}). The dashed line represents the linear fit for the content of Al and Me^{n+}.

However, the contents of Al and Me^{n+} in certain samples do not strictly conform to the inverse linear relationship, with some samples exhibiting significant deviations. These deviations may be attributed to ionic substitutions in the crystal lattice sites of chrysoberyl, specifically where Fe ions may not only substitute for octahedrally coordinated Al^{3+} but also potentially substitute for tetrahedrally coordinated Be^{2+}. Similarly, B ions can substitute not only for tetrahedrally coordinated Be^{2+} but also for octahedrally coordinated Al^{3+} [22,23]. Furthermore, the occupancy of trace element ions within different [AlO_6] octahedrons and [BeO_4] tetrahedrons in chrysoberyl remains uncertain and requires further clarification through specialized studies. A common source of trace elements in some crystals is nano-inclusions. For instance, previous studies have reported the presence of rutile inclusions within natural chrysoberyl, occurring in needle-like or platelet forms with particle sizes ranging from micrometers to nanometers [24,25]. This phenomenon may also have an impact on the concentration of trace elements.

There exists a clear positive correlation between the Fe concentration and the Me^{n+} concentration in chrysoberyl samples. Across samples from different origins, the positive correlation between Fe and Me^{n+} concentration remains robust (Figure 6A). In chrysoberyl samples, Fe comprises the largest proportion among the Me^{n+} elements, suggesting that Fe is a prominent octahedral site-substituting metal ion in chrysoberyl. Consequently, the substitution trend of Fe is generally similar to that of Me^{n+}. Furthermore, a moderate positive correlation is observed between the Ti concentration and the Me^{n+} concentration in chrysoberyl samples, indicating that Ti ions exhibit a somewhat similar substitution trend to Me^{n+} (Figure 6B).

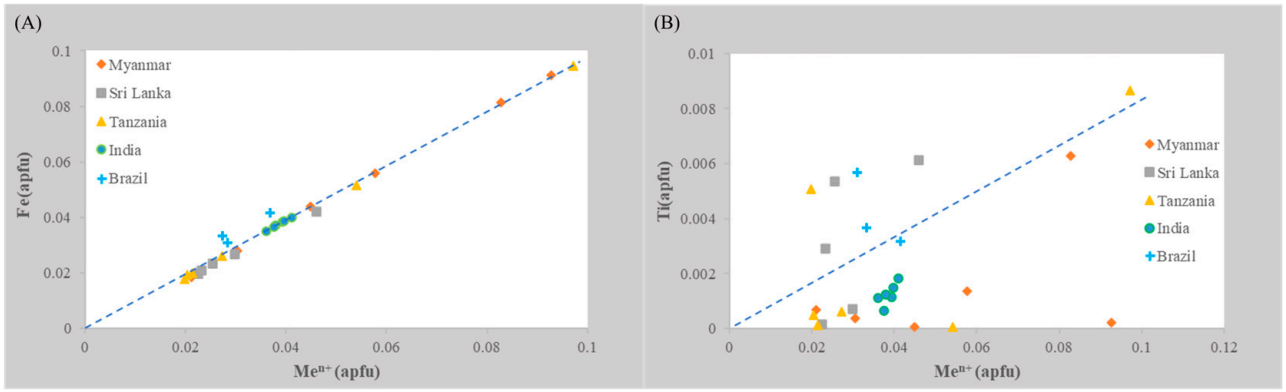


Figure 6. The relationship between trace elements and Me^{n+} concentration in chrysoberyl samples. (**A**) The relationship between Me^{n+} and Fe. The dashed line represents the linear fit for the content of Fe and Me^{n+}; (**B**) the relationship between Me^{n+} and Ti. The dashed line is the approximation of the content of Ti and Me^{n+}.

4.3. The Role of Trace Elements in Photoluminescence and Coloration

By using LA–ICP–MS and PL spectroscopy, the presence of trace elements related to luminescence, i.e., Cr, in the chrysoberyl samples was confirmed. However, the role of these trace elements in photoluminescence and coloration remains to be elucidated.

Sample S3, which exhibits color zoning, serves as an exemplary case to illustrate the spatial correlation between photoluminescence and coloration. Initially, within the color-zoned regions, LA–ICP–MS measurements were performed at three points across three distinct vertical zones, and the concentrations obtained were averaged. Analysis of the compositions across these different color zones revealed minor discrepancies but generally consistent results (Table 2). Furthermore, UV–Vis–NIR absorption spectra were also acquired in situ, in proximity to the LA–ICP–MS measurement points across different sections of the color zoning. The specific areas for spectrum acquisition are depicted in the inset of Figure 7. Quantifying the color using CIE L*a*b* coordinates [26] revealed that the darker sections of the generated color patches contained more red hue. When considered alongside the aforementioned PL spectrum, it is conceivable that the sample contains a trace amount of Cr. According to prior literature [6,27], Cr^{3+} in alexandrite exhibits an absorption peak around 410 nm, a band near 576 nm, and a sharp absorption line at 680 nm. However, these absorption features of Cr^{3+} are not prominently displayed in chrysoberyl. Therefore, a PL mapping was conducted in the color-zoned area, and the results (Figure 8) showed intensity zoning that basically aligns with the position of the color zoning. A strong positive correlation was observed between the sharp peak series at 678 and 680 nm, indicating that these two peaks are related to the same origin. Specifically, compared to the lighter sections, the darker ones contain a higher concentration of Cr, despite the concentration of Cr in all analyzed regions of this sample falling below the detection limit of LA–ICP–MS. Additionally, the PL mapping intensity zoning generally aligns with the positions of the color bands. This is likely the reason for the color zoning in chrysoberyl, and it also demonstrates a spatial consistency between photoluminescence and coloration.

Table 2. Trace elements of chrysoberyl sample S3 in ppma.

		B	Fe	Ti	Cr	V	Ga	Sn
Section D	**P1**	66	3854	88	Bdl *	bdl	348	134
	P2	48	3701	91	bdl	bdl	339	130
	P3	48	3688	92	bdl	bdl	325	129
	Average	**54**	**3748**	**90**	**bdl**	**bdl**	**337**	**131**
Section M	**P4**	**75**	3977	117	bdl	bdl	332	115
	P5	61	3927	121	bdl	bdl	321	111
	P6	61	4037	120	bdl	bdl	318	113
	Average	**66**	**3980**	**119**	**bdl**	**bdl**	**324**	**113**
Section L	**P7**	78	3721	90	bdl	bdl	318	76
	P8	73	3620	94	bdl	bdl	308	76
	P9	73	3882	93	bdl	bdl	304	91
	Average	**75**	**3741**	**92**	**bdl**	**bdl**	**310**	**81**

* bdl = below the detection limit of the LA-ICP-MS analysis.

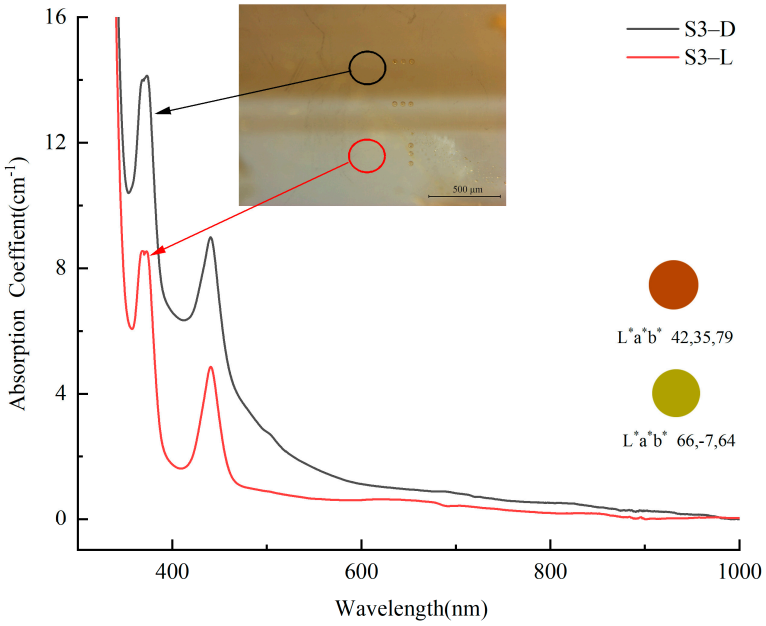


Figure 7. The UV–Vis–NIR spectra of chrysoberyl sample S3. CIE L*a*b* coordinates of color circles here are calculated under D65 light for a 1 cm wafer thickness to demonstrate color features of chrysoberyl at the different sections of the zoning.

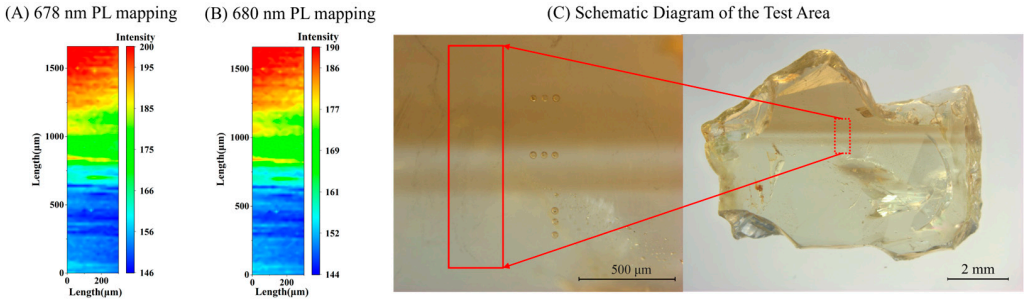


Figure 8. Laser PL mapping of chrysoberyl sample S3: (**A**) at 678 nm; (**B**) at 680 nm; (**C**) schematic diagram of the test area.

5. Conclusions

In this work, twenty-six chrysoberyl samples originating from various localities were investigated by LA–ICP–MS, PL spectroscopy, and UV–Vis–NIR spectroscopy. The chemical

analysis revealed the primary trace elements present in chrysoberyl are Fe, Ti, Ga, Sn, B, Cr, and V. Nearly all samples contained these trace elements, albeit with varying relative concentrations. Isomorphic substitution of ions frequently occurs at lattice sites within the chrysoberyl structure. Specifically, Al in octahedral sites is predominantly substituted by transition metal ions and other ions, collectively denoted as Me^{n+}, which primarily encompass Fe, Ti, Cr, V, Ga, and Sn.

The PL spectra exhibit a doublet of sharp peaks centered at 678 and 680 nm, which are attributed to Cr^{3+} ions. The PL spectrum characterized the presence of Cr concentration below the detection limit of LA–ICP–MS, thereby demonstrating the high sensitivity of PL spectroscopy.

The UV–Vis–NIR spectra of chrysoberyl samples revealed clear absorption bands attributed to Fe. Combined with LA–ICP–MS analysis and PL mapping of sample S3, which exhibits color zoning, the darker sections were found to contain a higher concentration of Cr, albeit the concentrations of Cr in this sample fell below the detection limit of LA–ICP–MS. The concentrations of other elements remained largely consistent. This indicates that subtle differences in Cr concentration may be the underlying cause of color zoning in chrysoberyl. Furthermore, this finding elucidates the spatial correlation between photoluminescence and coloration, offering new technical methods and perspectives for exploring the origin of color zoning in such gemstones.

Author Contributions: Conceptualization, L.D.; methodology, L.D.; validation, L.D., Y.L. and X.G.; writing—original draft preparation, L.D.; writing—review and editing, R.L. All authors have read and agreed to the published version of the manuscript.

Funding: This research received no external funding.

Data Availability Statement: The article contains all relevant data.

Acknowledgments: The authors would like to thank Jia Liu and Xing Xu for their help in measurements.

Conflicts of Interest: The authors declare no conflicts of interest.

References

1. Ferraz, G.M.; Watanabe, S.; Souza, S.O.; Scalvi, R.M.F. TL, EPR and optical absorption studies on natural alexandrite compared to natural chrysoberyl. *Radiat. Prot. Dosim.* **2002**, *100*, 471–474. [CrossRef]
2. Schmetzer, K.; Malsy, A.K. Natural alexandrite with an irregular growth pattern: A case study. *J. Gemmol. Assoc. Hong Kong* **2011**, *32*, 68–75.
3. Schmetzer, K.; Bernhardt, H.J.; Gilg, H.A. Characterization of Oriented Inclusions in Cat's-eye, Star and Other Chrysoberyls. *J. Gemmol.* **2016**, *35*, 28. [CrossRef]
4. Sun, Z.; Palke, A.C.; Muyal, J.; McMurtry, R.; Materials, P. How to facet gem-quality chrysoberyl: Clues from the relationship between color and pleochroism, with spectroscopic analysis and colorimetric parameters. *Am. Miner.* **2017**, *102*, 1747–1758. [CrossRef]
5. Schmetzer, K. Pleochroism and color change in faceted alexandrite: Influence of cut and sample orientation. *Gems Gemol.* **2019**, *55*, 61–71. [CrossRef]
6. Farrell, E.; Newnham, R.; Materials, P. Crystal-field spectra of chrysoberyl, alexandrite, peridot, and sinhalite. *Am. Mineral.* **1965**, *50*, 1972–1981.
7. Jyothi, S.S.; Rani, G.P.; Venkateswarulu, P.; Rao, R.V.; Rautray, T.R. Elemental Analysis of Indian Natural Chrysoberyl Gem-Stones by PIXE Technique. In *Recent Advances in Material Sciences: Select Proceedings of ICLIET 2018*; Springer: Singapore, 2019; p. 297–317.
8. Gao, Y.; Li, X.; Cheng, Y.; Huang, T.; Li, K.; Xu, B.; Tang, R. Gemological, Spectral and Chemical Features of Canary Yellow Chrysoberyl. *Crystals* **2023**, *13*, 1580. [CrossRef]
9. Jochum, K.P.; Nohl, U.; Herwig, K.; Lammel, E.; Stoll, B.; Hofmann, A.W. GeoReM: A new geochemical database for reference materials and isotopic standards. *Geostand. Geoanalytical Res.* **2005**, *29*, 333–338. [CrossRef]
10. Liu, Y.; Hu, Z.; Gao, S.; Günther, D.; Xu, J.; Gao, C.; Chen, H. In situ analysis of major and trace elements of anhydrous minerals by LA-ICP-MS without applying an internal standard. *Chem. Geol.* **2008**, *257*, 34–43. [CrossRef]
11. Emmett, J.L.; Scarratt, K.; McClure, S.F.; Moses, T.; Douthit, T.R.; Hughes, R.; Novak, S.; Shigley, J.E.; Wang, W.; Bordelon, O.; et al. Beryllium diffusion of ruby and sapphire. *Gems Gemol.* **2003**, *39*, 84–135. [CrossRef]
12. Dubinsky, E.V.; Stone-Sundberg, J.; Emmett, J.L. A quantitative description of the causes of color in corundum. *Gems Gemol.* **2020**, *56*, 1–27. [CrossRef]

13. Ollier, N.; Fuchs, Y.; Cavani, O.; Horn, A.H.; Rossano, S. Influence of impurities on Cr^{3+} luminescence properties in Brazilian emerald and alexandrite. *Eur. J. Miner.* **2015**, *27*, 783–792. [CrossRef]
14. Powell, R.C.; Xi, L.; Gang, X.; Quarles, G.J.; Walling, J.C. Spectroscopic properties of alexandrite crystals. *Phys. Rev. B* **1985**, *32*, 2788–2797. [CrossRef]
15. Forbes, C.E. Analysis of the spin-Hamiltonian parameters for Cr^{3+} in mirror and inversion symmetry sites of alexandrite (Al2−xCrxBeO4). Determination of the relative site occupancy by EPR. *J. Chem. Phys.* **1983**, *79*, 2590–2599. [CrossRef]
16. Ferguson, J.; Fielding, P. The origins of the colours of natural yellow, blue, and green sapphires. *Aust. J. Chem.* **1972**, *25*, 1371–1385. [CrossRef]
17. Emmett, J.L.; Atikarnsakul, U.; Stone-Sundberg, J.; Sangsawong, S. Yellow Sapphire: Natural, Heat-Treated, Beryllium-Diffused, and Synthetic. *Gems Gemol.* **2023**, *59*, 268–297. [CrossRef]
18. Kanouo, N.S.; Ekomane, E.; Yongue, R.F.; Njonfang, E.; Zaw, K.; Changqian, M.; Ghogomu, T.R.; Lentz, D.R.; Venkatesh, A.S. Trace elements in corundum, chrysoberyl, and zircon: Application to mineral exploration and provenance study of the western Mamfe gem clastic deposits (SW Cameroon, Central Africa). *J. Afr. Earth Sci.* **2016**, *113*, 35–50. [CrossRef]
19. Schmetzer, K.; Malsy, A.-K. Alexandrite and colour-change chrysoberyl from the Lake Manyara alexandrite-emerald deposit in northern Tanzania. *J. Gemmol.* **2011**, *32*, 179–209. [CrossRef]
20. Merino, E.; Villaseca, C.; Orejana, D.; Jeffries, T. Gahnite, chrysoberyl and beryl co-occurrence as accessory minerals in a highly evolved peraluminous pluton: The Belvís de Monroy leucogranite (Cáceres, Spain). *Lithos* **2013**, *179*, 137–156. [CrossRef]
21. Franz, G.; Morteani, G. Be-minerals: Synthesis, stability, and occurrence in metamorphic rocks. *Rev. Miner. Geochem.* **2002**, *50*, 551–589. [CrossRef]
22. See, R.F.; Kruse, R.A.; Strub, W.M. Metal-ligand bond distances in first-row transition metal coordination compounds: Coordination number, oxidation state, and specific ligand effects. *Inorg. Chem.* **1998**, *37*, 5369–5375. [CrossRef]
23. Chen, J.Z.; Yang, J.H.; Wang, Q.L. The Principle of Constructing the Crystal Structures of Nigerite-Taaffeite-Hogbomite and Their Related Minerals. *Acta. Mineral. Sinica.* **2001**, *21*, 19–26.
24. Drev, S.; Komelj, M.; Mazaj, M.; Daneu, N.; Rečnik, A. Structural investigation of (130) twins and rutile precipitates in chrysober-yl crystals from Rio das Pratinhas in Bahia (Brazil). *Am. Mineral.* **2015**, *100*, 861–871. [CrossRef]
25. Peucat, J.; Ruffault, P.; Fritsch, E.; Coz, M.B.-L.; Simonet, C.; Lasnier, B. Ga/Mg ratio as a new geochemical tool to differentiate magmatic from metamorphic blue sapphires. *Lithos* **2007**, *98*, 261–274. [CrossRef]
26. Corbala´n, M.; Milla´n, M.S.; Yzuel, M.J. Color pattern recognition with CIELAB coordinates. *Opt. Eng.* **2002**, *41*, 130–138.
27. Walling, J.; Peterson, O.; Jenssen, H.; Morris, R.; O'Dell, E. Tunable alexandrite lasers. *IEEE J. Quantum Electron.* **1980**, *16*, 1302–1315. [CrossRef]

Disclaimer/Publisher's Note: The statements, opinions and data contained in all publications are solely those of the individual author(s) and contributor(s) and not of MDPI and/or the editor(s). MDPI and/or the editor(s) disclaim responsibility for any injury to people or property resulting from any ideas, methods, instructions or products referred to in the content.